

*Annual Review of Condensed Matter Physics*  
**Experimental Progress in  
 Superconducting Nickelates**

Bai Yang Wang,<sup>1,2</sup> Kyuho Lee,<sup>1,2,3</sup> and Berit H. Goodge<sup>4</sup>

<sup>1</sup>Stanford Institute for Materials and Energy Sciences, SLAC National Accelerator Laboratory, Menlo Park, California, USA; email: bwang87@stanford.edu, kyuholee@stanford.edu

<sup>2</sup>Department of Applied Physics, Stanford University, Stanford, California, USA

<sup>3</sup>Current affiliation: Department of Physics, Massachusetts Institute of Technology, Cambridge, Massachusetts, USA; email: kyuholee@mit.edu

<sup>4</sup>Max Planck Institute for Chemical Physics of Solids, Dresden, Germany; email: berit.goodge@cpfs.mpg.de

ANNUAL  
REVIEWS **CONNECT**

[www.annualreviews.org](http://www.annualreviews.org)

- Download figures
- Navigate cited references
- Keyword search
- Explore related articles
- Share via email or social media

Annu. Rev. Condens. Matter Phys. 2024. 15:305–24

First published as a Review in Advance on  
 December 5, 2023

The *Annual Review of Condensed Matter Physics* is  
 online at [conmatphys.annualreviews.org](http://conmatphys.annualreviews.org)

<https://doi.org/10.1146/annurev-conmatphys-032922-093307>

Copyright © 2024 by the author(s). This work is licensed under a Creative Commons Attribution 4.0 International License, which permits unrestricted use, distribution, and reproduction in any medium, provided the original author and source are credited. See credit lines of images or other third-party material in this article for license information.



### Keywords

unconventional superconductivity, layered nickelates, thin films, charge order, strange metal

### Abstract

The superconducting nickelates were first proposed as potential analogs to the cuprate unconventional superconductors in 1999, but it took twenty years before superconductivity was successfully stabilized in epitaxial thin films. Since then, a flurry of both experimental and theoretical efforts have sought to understand the similarities and differences between the two systems and how they manifest in the macroscopic superconducting and normal state properties. Although the nickelates and cuprates indeed share many commonalities within their respective phase diagrams, several notable differences have also emerged, especially regarding their parent compounds, electronic hybridization, and fermiology. Here, we provide a survey of the rapidly developing landscape of layered nickelate superconductors, including recent experimental progress to probe not just the superconducting but also normal state and other ordered phases stabilized in these compounds.

## 1. INTRODUCTION

### 1.1. A Brief History of Superconducting Nickelates

The discovery of superconducting copper oxides (cuprates) in 1986 by Bednorz & Müller (1) motivated a search for analogous unconventional superconductivity in other material systems. With nickel adjacent to copper in the periodic table, the layered monovalent nickel oxide (nickelate) systems such as infinite-layer (IL)  $\text{RNiO}_2$  ( $\text{R}$  = trivalent rare-earth; **Figure 1a**) were long considered a promising candidate (2). Following many experimental endeavors, in 2019 Li et al. were finally able to realize superconductivity in hole-doped  $\text{Nd}_{0.8}\text{Sr}_{0.2}\text{NiO}_2$  thin films (3) by first growing epitaxial perovskite precursor  $\text{Nd}_{0.8}\text{Sr}_{0.2}\text{NiO}_3$  on  $\text{SrTiO}_3$  and using  $\text{CaH}_2$ -assisted soft-chemistry reduction to deintercalate the apical oxygens, thereby reaching the IL phase. The family of superconducting nickelates has since expanded to include IL La- and Pr-based compounds (referred to below as La- and Pr-nickelates) substitutionally doped with Sr or Ca (4–6), as well as quintuple-layer (QL)  $\text{Nd}_6\text{Ni}_5\text{O}_{12}$ , which stabilizes a similar formal electron count (7, 8). Superconductivity up to almost 80 K was also subsequently demonstrated in the bilayer perovskite compound  $\text{La}_3\text{Ni}_2\text{O}_7$  under high pressure (14–43.5 GPa) (9, 10), though current understanding of these two families points toward rather distinct pictures of superconductivity.

In this article, we focus on experimental progress in the layered square-planar compounds,  $\text{R}_{n=1}\text{Ni}_n\text{O}_2$  ( $n = 5, \infty$ ). Their breakthrough launched significant efforts to rapidly characterize the growing family of layered nickelates, with a natural emphasis on comparison to the cuprates (9). Indeed, the emerging electronic phase diagram of hole-doped nickelates shares many broad similarities to that of the cuprates (**Figure 1b**), including a doping-dependent superconducting dome, regions of  $T$ -linear and  $T^2$  resistivity, and signatures of charge order and other ordered phases (10, 11, 14–16). In parallel, important differences have also been noted, particularly regarding the metallicity of the parent compound and effects of reduced hybridization between metal and oxygen states in the nickelates (17, 18). This imperfect overlap between two closely

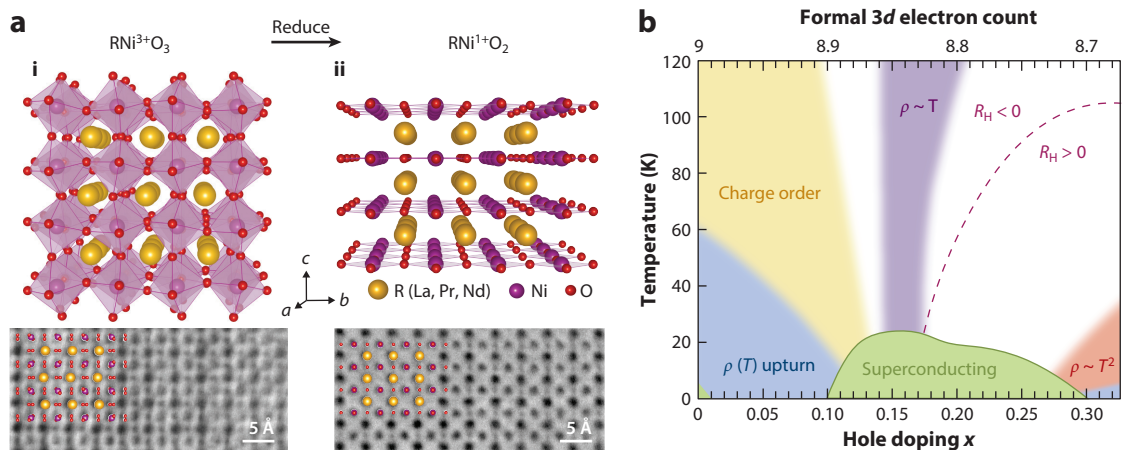


**Figure 1**

(a) Basic crystal structure of (i) the precursor perovskite and (ii) reduced infinite-layer nickelates, with annular bright-field scanning transmission electron microscopy images showing the removal of apical oxygens from the R planes. Lattice vectors are indicated in the pseudocubic convention. (b) Schematic representation of the known hole-doping phase diagram based on experimental reports so far (5, 10–13). Regions with characteristic temperature ( $T$ )-dependent resistivity ( $\rho$ ) behavior are indicated with blue, purple, and red shading. The approximate crossover in Hall resistance ( $R_H$ ) is marked by a dashed line. Further experiments are needed to establish the doping dependence of charge-ordered phases.

analogous systems provides tantalizing potential to better understand the underlying mechanism of unconventional superconductivity in both. Here, we aim to provide a brief overview of the current experimental progress in the layered nickelates (18–27), as well as to identify both pressing and promising avenues of inquiry for future work.

## 1.2. Overview of the Crystal and Electronic Structure

The IL crystal structure  $ABO_2$  (**Figure 1a**) is the simplest primary atomic motif of the superconducting cuprates, namely square-planar  $BO_2$  planes separated by A-site spacer planes (2). In  $RNiO_2$ , nickel takes on a formal  $1+$  valence and a  $d^9$  electron count, which can be electronically doped to stabilize superconductivity. Similar to cuprates, nickelates exhibit a dome in the superconducting transition temperature  $T_c$  in the hole-doped phase diagram that extends (at the time of writing) from approximately  $x = 0.1$ – $0.3$  hole doping, with optimal doping considered near  $x = 0.15$ – $0.20$  (5, 10, 12, 13) (**Figure 1**). The superconducting nickelate family also includes the related QL compound  $Nd_6Ni_5O_{12}$  (7) (Section 2.4); for clarity, we refer to the combined family simply as layered nickelates.

At first glance, the structural and electronic similarities as well as the observation of superconductivity and a hole-doped superconducting dome argue for a strong analogy between the nickelates and the cuprates. However, there exist important distinctions between the two systems, particularly in the orbital alignment and the fermiology (17). Although the larger on-site Coulomb repulsion ( $U$ ) compared to the charge-transfer gap ( $\Delta$ ) puts the cuprates in the charge-transfer regime of the Zaanen–Sawatzky–Allen framework (28), the  $d^9$  covalency is reduced by the smaller nuclear charge in the nickelates (29–32) such that the charge-transfer energy is larger than the Coulomb repulsion ( $\Delta > U$ ), pushing the nickelates toward the Mott–Hubbard regime (33–35) (**Figure 2a**). This distinction in the band alignment also results in stronger hybridization between Ni  $3d$  and R  $5d$  bands and additionally forms two self-doped electron pockets on top of the cuprate-like  $d_{x^2-y^2}$  hole bands in the Fermi surface (**Figure 2d**), making the

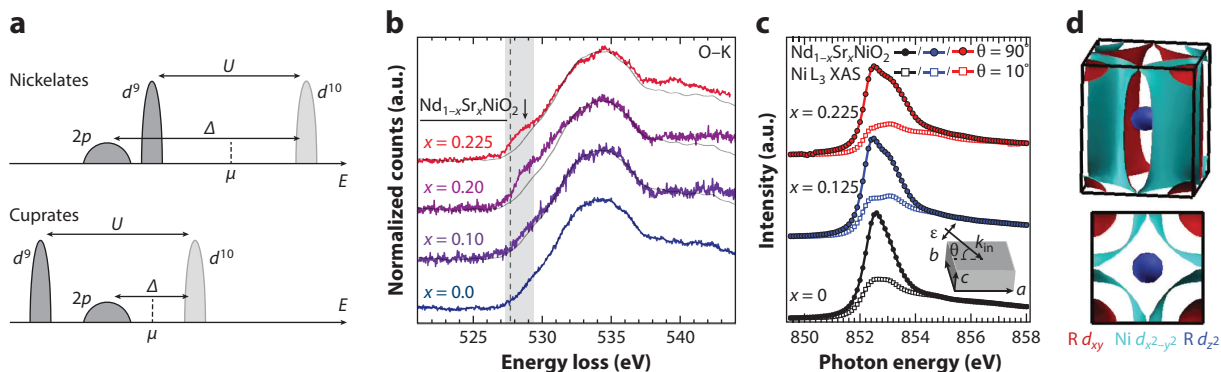


**Figure 2**

(a) Schematic Zaanen–Sawatzky–Allen (28) electronic structure comparison between the IL nickelates and cuprates, showing the oxygen  $2p$  and metal (Ni or Cu)  $3d$  states illustrating the increase in nickelate charge-transfer energy  $\Delta$  relative to the Coulomb repulsion  $U$ . (b,c) Hole doping via Sr-substitution  $x$  in  $Nd_{1-x}Sr_xNiO_2$  films results in core-level spectral responses involving both the O  $2p$  and Ni  $3d$  states. The emergent prepeak on the O–K edge is reminiscent of the Zhang–Rice singlet peak observed in hole-doped cuprates, whereas the broadening of the Ni– $L_{2,3}$  edge suggests multiband hole interactions. (d) Schematic representation of an IL nickelate Fermi surface, showing the Ni  $d_{x^2-y^2}$  hole and R  $d_{2,2}$  and  $d_{xy}$  electron pockets. Panels a and b adapted from Reference 34 (CC BY-NC-ND 4.0). Panel c adapted with permission from Reference 36. Panel d adapted from Reference 37 (CC BY 4.0). Abbreviation: IL, infinite-layer.

nickelates an intrinsically multiband system (2, 17, 32, 35, 37–51). Furthermore, the hybridization between O  $2p$  and metal  $3d$  is significantly reduced in the nickelates (33–35) such that the doped holes are found in both the O ligand band (34) and the Ni  $3d$  band (36, 52) (**Figure 2b,c**). A central question is how these distinctions manifest in the macroscopic superconducting nature of the nickelates, the understanding of which can potentially further elucidate the underlying mechanism of unconventional superconductivity in the two systems.

The layered atomic structure of superconducting nickelates suggests strongly anisotropic electronic behavior, such that they can be considered quasi-two-dimensional (quasi-2D). This is thus far consistent with experimental measurements of in-plane ( $\xi_{\parallel}$ ) and estimates of out-of-plane ( $\xi_{\perp}$ ) coherence lengths (3, 5, 6, 53–58) (see Section 3.1), although further experimental verification is needed. This picture may be subtly modified, however, by the self-doping mechanism mentioned above. Experimentally, signs of doped hole interactions with the R  $5d$  bands have been directly observed through local core-level spectroscopy (34), but more concrete clarification about the role of the R bands and distinctions between the various cation species remain to be demonstrated. The multilayered compounds (7) may further offer a route to more precisely tune the effective dimensionality of this system, as would certain heterostructure (59) or other thin-limit synthesis approaches (60, 61). Direct out-of-plane transport measurement enabled by further improvements in bulk synthesis or  $a$ -axis-oriented thin film growth (62) will be illuminating, although experimentally challenging.

## 2. SYNTHESIS CHALLENGES

Many of the unaddressed or debated properties of the layered nickelates remain so due to outstanding challenges associated with the synthetic limitations of these compounds, which can be divided into two categories. First is the difficulty of achieving highly crystalline, single-phase layered square-planar samples due to the low thermodynamic stability of monovalent nickel. This encompasses two further material challenges: first, the nontrivial inclusion of structural defects, which yield significant variations in the electrical conductivity and hamper the observation of inherent electrical transport properties (10, 12, 13, 63–65), and second, the vulnerability of the film surface to degradation or secondary-phase formation during the topotactic reduction step (7, 62, 63, 66) and to reoxidation afterward (62, 67), making surface-sensitive measurements such as angle-resolved photoemission spectroscopy (ARPES) (35, 68) or scanning tunneling spectroscopy difficult (69, 70). Although the former can hopefully be resolved with continued efforts in crystallinity improvements (10, 63, 71–73), the latter is expected to require more careful experimental design to access the pristine  $\text{II}$  surface.

Second is the unavailability, at the time of writing, of bulk superconducting layered nickelate samples. With large critical current density ( $J_c$ ) (see Section 3.1) and the alleviation of polar discontinuity via interface reconstruction (74) suggesting that the nickelate superconductivity observed in thin films is indeed a bulk response rather than an interface effect, the absence of superconductivity in bulk samples thus far is largely attributed to limited crystallinity due to additional materials challenges in bulk synthesis (13, 72, 73, 75) (see Section 2.3), although intrinsic strain effects might still be relevant (38). This currently limits the experimental measurements to thin film geometry, yielding various complications arising from the substrate and (when present) capping layer and precluding measurements requiring large sample volume such as neutron scattering.

### 2.1. Topotactic Reduction

$\text{Ni}^{1+}$  is thermodynamically unstable, such that natural oxides with 1+ valence (the desired  $d^9$  configuration) are uncommon and synthetically challenging. The successful approach thus far has

been to first synthesize more stable phases (e.g.,  $\text{Ni}^{3+}$ ), followed by topotactic chemical reaction to selectively remove some oxygen from the structure, thereby reducing the nickel valence. Synthesis of IL  $\text{LaNiO}_2$  by this approach using  $\text{H}_2$  gas as the reduction reagent was already reported before the predictions of superconductivity (76). Ultimately, metal hydrides such as  $\text{NaH}$  (77, 78) and  $\text{CaH}_2$  (79) were found to more reproducibly yield IL nickel oxides, with efforts primarily focused on  $\text{LaNiO}_2$  expanding to  $\text{NdNiO}_2$  (66, 78) and paving the way for the doped superconducting compounds (3). Aluminum is also a viable alternative as the reduction reagent (80, 81).

Several important questions about the mechanism and uniformity of oxygen deintercalation in reduced nickelate samples remain to be explored in greater detail. In particular, both bulk structural measurements and local spectroscopic probes (34) have indicated various levels of nanoscale oxygen inhomogeneity within many fully reduced nickelate samples, although measurements across longer length scales ( $\gtrsim 50$  nm) suggest the macroscopic distribution is largely homogeneous (82). It is also an open question if oxygen doping—in which the electronic doping is achieved by controlling the oxygen stoichiometry ( $\text{RNiO}_{2+\delta}$ )—is possible in the IL nickelates as in some cuprate systems (83, 84) or whether it is forbidden due to a closely competing  $\text{RNiO}_{2.5}$  phase (67). More concretely establishing the precise oxygen stoichiometry and distribution in these compounds has important implications for understanding both the electronic structure (see Section 2.4) and competition or coexistence with other local ordered phases (see Section 5).

## 2.2. Balancing Epitaxial Strain in Thin Films

The synthetic route to layered nickelates carries a twofold challenge to balance the epitaxial strain. In particular, the choice of the substrate is significantly complicated by a large expansion of the in-plane lattice constant from the as-grown to the reduced phase: Substrates that are well lattice-matched to the precursor will impart very high compressive strain on the layered phase, whereas substrates that are better matched to the layered phases require growing the precursors under high tensile strain conditions (63, 85). The first superconducting samples demonstrated success with the latter approach using  $\text{SrTiO}_3$  substrates, which are a close lattice match to  $\text{NdNiO}_2$  and related compounds (3). The tensile strain conditions of the perovskite growth, however, resulted in high densities of lattice strain-relieving defects, particularly vertical Ruddlesden–Popper-type faults, in all reported samples (12, 13). Crystallinity improvements were achieved with careful optimization of the perovskite phase growth conditions (63), whereas mitigating strain effects by growing the perovskite precursors under lower tensile strain, e.g., increasing the film lattice constant (5) or decreasing the substrate lattice constant (10, 86), leads to major leaps in the sample quality. This concept of a Goldilocks zone for epitaxial strain was similarly demonstrated in the layered square-planar compounds (85). Overcoming strain relaxation will be required to increase sample thickness beyond the current limit of  $\sim 15$  nm for superconducting IL samples. As a complement to studies of the electronic evolution in the thin limit (60), this will enable a more concrete establishment of the critical thickness above which physical properties can be regarded as bulk-like.

## 2.3. Bulk Crystals

Thus far, the synthesis of superconducting bulk nickelates remains elusive (71–73, 87, 88). This initially resulted in different interpretations of the superconductivity observed in thin films, raising the question of interfacial superconductivity (89, 90). Experimental investigations of the nickelate– $\text{SrTiO}_3$  interface, however, revealed a single unit cell intermediate layer atomic reconstruction, ruling out the possibility of interfacial effects driven by polar discontinuity as the primary driver of observed superconductivity in these systems (74). Rather, the key differences between thin films and bulk single crystals seem to be: (a) the large surface-to-volume ratio in thin films compared

to single crystals (79) and (b) the presence of an epitaxial template with the substrate (and in some cases a capping layer) (63, 67, 85, 91). The former may play a role in the time and resulting uniformity of the topotactic oxygen reduction: Single crystals typically require much longer reduction times than thin films of similar compounds (63, 72), although the microscopic details of this process have not yet been systematically explored.

The latter effect can be further broken into two considerations including possible band modifications due to the epitaxial strain imposed on the film (38, 85) and the promotion of single-phase orientation (85). Local measurements of reduced bulk crystals show promising progress toward the characteristics observed in thin films of the same compounds (72), but individual crystals are subject to the formation of and subsequent fracturing along microscale orthogonal crystalline domains. By contrast, thin films exhibit predominantly single-domain orientation, with some examples of local lattice reorientation in cases of large compressive strain in the reduced phase (5, 67, 85, 92). It therefore seems likely that a key contribution of the substrate is not just mechanical support but also predefinition of the layered  $a$ - $b$  plane to preferentially form single domains in the reduced sample. Reproducing similar effects in bulk single crystals through appropriate symmetry breaking or applied external stress may thus be a fruitful route for synthetic improvement in the future.

## 2.4. Doping Strategies

To date, the primary method for hole doping the nickelate parent compounds is through substitutional cation doping of alkali metals (Sr or Ca) on the R site. Encouragingly, reports from independent groups are in generally good agreement regarding the relative doping-dependent properties (12, 13), but precise and absolute quantification of the elemental substitution and corresponding hole doping remains challenging. Because the oxygen concentration in these compounds is used to tune the formal nickel valence, off-stoichiometry in the form of excess oxygen could contribute additional holes and shift the absolute values of the currently understood doping phase diagram to higher  $x$ . The use of metal hydrides for topotactic reduction in many samples has also raised questions about the role of hydrogen, including suggestions of hydrogen-incorporated phases (93–95) and hydrogen-induced doping effects (96). Ding et al. (96) report a strong correlation between superconductivity and metrics of hydrogen incorporation in their films, whereas bulk neutron scattering studies of  $\text{LaNiO}_2$  (72, 73) and thin film secondary-ion mass spectroscopy studies of  $\text{NdNiO}_2$  (66) suggest that the majority of excess hydrogen resides in the decomposed and secondary-phase regions of the samples, arguing against any significant role of hydrogen in both the structural and electronic aspects of the IL nickelates. Precise quantification of elemental stoichiometry across many samples is therefore a high priority.

Thus far, elemental characterization has not detected any signs of significant cation order (4, 5, 34, 72), but more investigations into the impact of (dis)order in the cation lattice may be enlightening, especially relating to other correlated phases (see Section 5). It has also been proposed that the dopant species may play a role in defining the effective superconducting dimensionality in nickelates due to the impact of ionic size fluctuations (61). It might be further possible to tune the stability of charge order by using a larger dopant such as barium, as has been the case for  $\text{La}_{2-x}\text{B}_x\text{CuO}_4$  (B = alkali metal dopant) (97, 98).

Alternative methods of achieving electronic doping and tuning dimensionality without the introduction of A-site cation disorder have also been pursued. Structural doping has been proposed through heterostructuring approaches based on alternating layers of nickelate and other oxide compounds (99–101), although experimental efforts thus far have yet to demonstrate superconductivity (59). The average nickel  $3d$  electron count can be tuned according to formal

valence-counting rules in different members of the layered square-planar homologous series  $R_{n+1}\text{Ni}_n\text{O}_{2n+2}$ , of which the (undoped) IL compounds are the  $n = \infty$  phase. As with the ILs, these layered compounds are synthesized first in the corresponding Ruddlesden–Popper phase ( $R_{n+1}\text{Ni}_n\text{O}_{3n+1}$ ) and subsequently reduced through a similar process of topotactic oxygen deintercalation (7, 102, 103). Following the emerging hole-doped phase diagram in IL nickelates (12, 13), the  $n = 5$  QL square-planar nickelates are near optimal doping with a formal Ni  $3d^{8.8}$  character, and they do indeed superconduct (7). More thorough exploration of this branch in the nickelate family tree (e.g., R species, complementary chemical and structural doping) will likely prove challenging but fruitful.

All of the doping schemes described so far have their own inherent limitations, including inevitable A-site disorder, discrete levels of doping, difficulties in the synthesis of higher doping levels, and underlying growth challenges associated with cation size mismatch. It will be beneficial to explore other possible routes for doping, such as electrostatic or ionic liquid gating; intercalation of ions such as lithium, fluorine, or hydrogen; and oxygen stoichiometry control. These methods will also open the door to possibilities of electron doping, which has been proposed as one possible route to realize superconductivity at even higher temperatures in trilayer compounds (104).

### 3. SUPERCONDUCTIVITY

The scientific interest in the layered nickelates thus far has been mainly driven by the comparison to their isostructural analog—the cuprate unconventional superconductors (2). As superconductivity emerges in both systems upon hole doping a square-planar-coordinated lattice of transition metal ions with  $3d^9$  electronic configuration, it is plausible to expect a shared unconventional nature of the superconducting phase. Simultaneously, the presence of the additional hybridized electron Fermi pockets driven by the R bands in the nickelates motivates an examination from the intermetallic superconductor perspective. In this sense, the nickelate superconductors may be a unique system that combines aspects of strong correlations related to doped Mott insulators and complex interplay between the R and Ni orbitals analogous to intermetallic/heavy-fermion superconductors (105–107).

#### 3.1. Energy Scale

Superconductivity is a macroscopic condensation of paired fermion quasiparticles with an order parameter characterized by its amplitude ( $\Delta$ ) and phase ( $\phi$ ). Substantial experimental progress has been made in clarifying the energy and length scales as well as the angular structure of these two physical quantities. Relating to the energy scale, two key quantities are the superconducting gap, characterizing the strength of Cooper pairing, and the superconducting phase stiffness, characterizing the energy cost of superconducting phase variations. Although the phase stiffness is usually orders of magnitude larger than the gap, a close interplay between the two can occur, as in cuprate superconductors (108).

So far, the superconducting gap of  $\text{Nd}_{0.8}\text{Sr}_{0.2}\text{NiO}_2$  ( $T_c \sim 13\text{--}15$  K, where  $T_c$  is defined as the onset temperature of the superconducting transition) has been examined by two experimental techniques. Performing single-particle tunneling measurements at 350 mK, Gu et al. (69) observed a V-shaped gap with a gap maximum ( $2\Delta$ ) of  $\sim 7.8$  meV =  $5.9 k_B T_c$  and a full gap of  $\sim 4.7$  meV =  $3.6 k_B T_c$ . Cervasio et al. (109) extracted a superconducting gap magnitude of  $2\Delta \sim 3.2$  meV =  $2.9 k_B T_c$  from terahertz reflectivity measurements using the Mattis–Bardeen model. Substantial synthesis progress, particularly to address limitations due to degradation of the sample top surface during topotactic reduction (70) (see Section 2), is likely needed before

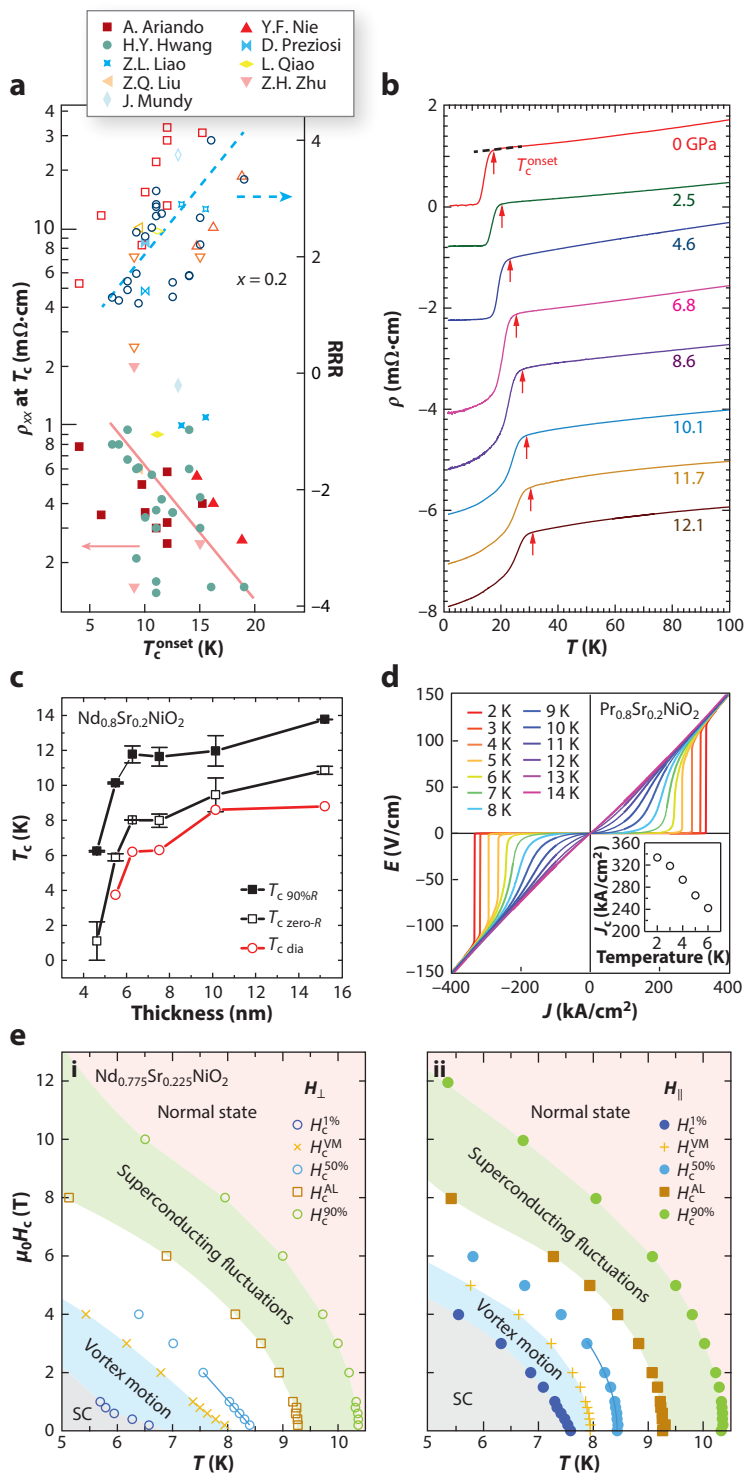
a quantitative agreement between the different measurement techniques can be achieved. An alternative route to measuring the superconducting gap using a planar tunneling technique could soon become viable following continuous refinement of the growth and reduction processes for oxide heterostructures involving IL or QL nickelates.

The other energy scale, the superconducting phase stiffness, is closely related to the superfluid density by the equation  $J_s(T) = (\hbar^2/\mu_0)(n_s \ell/m^*)$ , where  $\hbar$  is the reduced Planck's constant,  $\mu_0$  is the vacuum permeability,  $n_s$  is the superfluid density,  $m^*$  is the electronic effective mass, and  $\ell$  is the longer of the distance between neighboring NiO<sub>2</sub> planes and the  $c$ -axis superconducting coherence length  $\xi_{\perp}$ . For thin film geometry,  $\ell$  can take on the value of the film thickness if it is shorter than  $\xi_{\perp}$ . To date,  $n_s$  of IL nickelates has only been extracted from the measured absolute value of magnetic penetration depth  $\lambda$  using the mutual inductance technique, connected by the relation  $n_s/m^* = (1/4\mu_0 e^2)(1/\lambda^2)$ , where  $e$  is the elementary charge. A surprisingly low  $n_s$ ,  $\sim 0.003$  carriers per unit cell, is found (110), translating to a superconducting phase stiffness on the same order of magnitude as the superconducting gap scale. This is in contrast to the estimated normal state carrier density of  $\sim 0.9$ – $2.5$  carriers per unit cell based on a single-band interpretation of the Hall coefficient data (the Hall resistance response is indeed linear against magnetic field up to 14 T) (10) or  $\sim 0.2$  carriers per unit cell based on chemical composition (the contribution from the R 5d bands has been calculated to be one order of magnitude smaller) (37). This brings into question the nature of the superconducting transition in the IL nickelates, where phase coherence could also play an important role in determining  $T_c$  (111). Although these measurements await further experimental confirmation, they promise a potential  $T_c$  enhancement if the phase coherence could be improved through reduced disorder or increased film thickness (**Figure 3c**) (60).

Experimentally, proxies of the superconducting energy scale are more accessible. Critical temperature, critical current density, and critical magnetic field have all been reported by independent groups (3–5, 10, 13, 53, 55–58, 61, 65, 92, 112–114). Among the three known R variants in the IL nickelates and the QL nickelate superconductor, as-grown  $T_c$  has so far reached up to  $\sim 23$  K (10). **Figure 3a** summarizes the correlation between  $T_c$  and the quality of samples reported in the literature, reflected by the low-temperature normal state resistivity (defined at the superconducting onset temperature) and the room-temperature to low-temperature resistivity ratio (RRR). As shown for the case of doping  $x = 0.2$ , a nonsaturating trend can be found in which higher RRR and lower residual resistivity correlate with higher  $T_c$ , hinting at the possibility of further  $T_c$  improvement. Reporting an enhancement of the onset  $T_c$  to  $\sim 31.2$  K by 12.1 GPa hydrostatic pressure (**Figure 3b**), Wang et al. (92) also suggested compressive strain as a promising route for increasing  $T_c$ , in agreement with some theoretical works (38). The concurrent broadening of the superconducting transition and lattice-scale crystalline reconstruction, however, highlight the competing interplay between intrinsic and extrinsic strain effects in this system.

$J_c$  has been reported for only the IL nickelates so far, varying from 170 kA/cm<sup>2</sup> up to 330 kA/cm<sup>2</sup> (**Figure 3c**) (3, 4). This value is surprisingly large, on the same order of magnitude as the depairing current density,  $J_c^{\text{depair}} = H_c/(3\sqrt{6}\pi\lambda) \sim 70$ – $370$  kA/cm<sup>2</sup>. This is unusual considering the small  $n_s$  observed and may reflect a strong vortex pinning potential. Here,  $\lambda$  is assumed to be  $\sim 750$  nm (110) and  $H_c$ , the thermodynamic critical field, is assumed to be in the range of 150 Oe to 800 Oe, as discussed below.

As the IL nickelates have been characterized as type-II superconductors (see Section 3.3), there are two critical magnetic field scales: the lower critical field ( $H_{c1}$ ), marking the creation of the first magnetic vortex, and the upper critical field ( $H_{c2}$ ), marking the loss of macroscopic superconductivity (115). Of the two,  $H_{c2}$  has been well characterized in IL nickelates (3, 5, 6, 53, 56, 58, 112, 113) (**Figure 3e**). Depending on the R element composition,  $H_{c2}$  can reach up to over 35 T and 3–4 times the weak-coupling conventional Pauli limit, defined as  $1.86T_c$  (116–118). Based on the



(Caption appears on following page)

**Figure 3** (Figure appears on preceding page)

(a) Low-temperature normal state resistivities (*closed shapes*, left axis) and RRR (*open shapes*, right axis) of nominally  $x = 0.2$  hole-doped nickelate superconductors as a function of the superconducting onset temperature. The red solid line and blue dashed line are guides to the eye. Legend denotes experimental groups (3–7, 10, 12, 15, 54–56, 58, 60, 61, 64, 65, 86, 112, 113). (b) Temperature-dependent resistivity of a  $\text{Pr}_{0.82}\text{Sr}_{0.18}\text{NiO}_2$  sample as a function of hydrostatic pressure. Curves are vertically shifted for clarity. (c) Thickness dependence of  $T_c$  in  $\text{Nd}_{0.8}\text{Sr}_{0.2}\text{NiO}_2$  thin films on  $\text{SrTiO}_3$ . (d) Electric field strength ( $E$ ) versus current density ( $J$ ) of a  $\text{Pr}_{0.8}\text{Sr}_{0.2}\text{NiO}_2$  sample and (*inset*)  $J_c$  as a function of temperature. (e)  $H_c - T$  phase diagrams of an  $\text{Nd}_{0.775}\text{Sr}_{0.225}\text{NiO}_2$  sample for magnetic fields (i) along the  $c$  axis and (ii) in the  $a$ - $b$  plane.  $H_c$  of different definitions are shown, with  $H_c^{x\%}$  corresponding to resistivities reaching  $x\%$  of the normal state value,  $H_c^{\text{VM}}$  corresponding to the onset of magnetic vortex motion, and  $H_c^{\text{AL}}$  corresponding to the critical field extracted from Aslamazov–Larkin fitting of the superconducting transition. Panel *b* adapted from Reference 92 (CC BY 4.0). Panel *c* adapted from Reference 60 (CC BY 4.0). Panel *d* adapted with permission from Reference 4; copyright 2020 American Chemical Society. Panel *e* adapted with permission from Reference 53. Abbreviation: RRR, room-temperature to low-temperature resistivity ratio.

temperature dependence of  $H_{c2}$ , two groups have attributed the scale of  $H_{c2}$  to the combination of orbital depairing and paramagnetic depairing effects, with the paramagnetic depairing effect playing a central role in (Nd, Sr)NiO<sub>2</sub> systems (53, 112). This is in contrast to most oxide superconductors in which the paramagnetic depairing effect only comes into play when the alternative is suppressed by geometric confinement (119). The identification of the paramagnetic depairing effect implies a singlet pairing nature of the superconducting phase. Combined with the clear violation of the weak-coupling Pauli limit observed in La- and Pr-nickelates (55, 61, 116), this further suggests a strong coupling nature of the superconductivity or a nontrivial spin-orbit coupling strength in the system. Several groups have additionally reported a clear dependence of the  $H_{c2}$  scale on the R element (55, 116, 120). Based on angular magnetoresistance (AMR) measurements and crystal field calculations, Wang et al. (116) attributed this dependence to the magnetic nature of the  $4f$  electrons associated with the R elements.

In contrast, experimental measurement of  $H_{c1}$  has only been reported once so far. Chow et al. (54) estimated  $H_{c1} \sim 79$  Oe for  $\text{Nd}_{0.8}\text{Sr}_{0.2}\text{NiO}_2$  based on field-dependent magnetization measurements. Combined with the knowledge of  $H_{c2}$ , this provides an estimate of  $H_c = (H_{c1}H_{c2})/(\ln\kappa) \approx 150$  Oe, where  $\kappa = \lambda/\xi \approx 750 \text{ nm}/4 \text{ nm} \approx 190$ . Another estimate could be made based on the measured  $\lambda \sim 750$  nm and  $\xi \sim 4$  nm:  $H_c = \Phi_0/(2\sqrt{2}\pi\lambda\xi) \approx 800$  Oe. Here,  $\Phi_0$  is the magnetic flux quantum. Despite the numerical discrepancy between the two estimates, it is reasonable to expect the actual field scale to be of a similar order of magnitude.

### 3.2. Superconducting Gap Symmetry

The angular structure of  $\Delta$  and  $\phi$  carries strong implications on the underlying pairing mechanism. Up to now, only the angular structure of  $\Delta$  has been probed by examining the low-temperature dependence of  $n_s$ : A fully opened gap results in an exponential saturation of  $n_s$  at temperatures below which the superconducting gap fully opens, whereas a nodal gap shows a continuing increase in  $n_s$ . As illustrated in **Figure 4a**, Harvey et al. (110) reported a nonsaturating quadratic increase of  $n_s$  in IL La- and Pr-nickelate samples at low temperatures and interpreted this as a signature of a nodal superconducting gap. The exponential saturation and unusual slight downturn of  $n_s$  seen in IL Nd-nickelates were interpreted as an artifact due to the complications coming from the  $\text{Nd}^{3+}$   $4f$  magnetic moments. Such a  $4f$  moment-driven distinction among the three R variants is not only reproduced by another  $n_s$  measurement using the tunnel-diode-oscillator setup (54) (illustrated in **Figure 4a**) but also seen in the  $H_{c2}$  data (see discussion in Section 3.1) and the AMR measurements (15, 57, 61, 116). Although IL La- and Pr-nickelates show twofold azimuthal AMR response (116), Nd-nickelates exhibit fourfold behavior

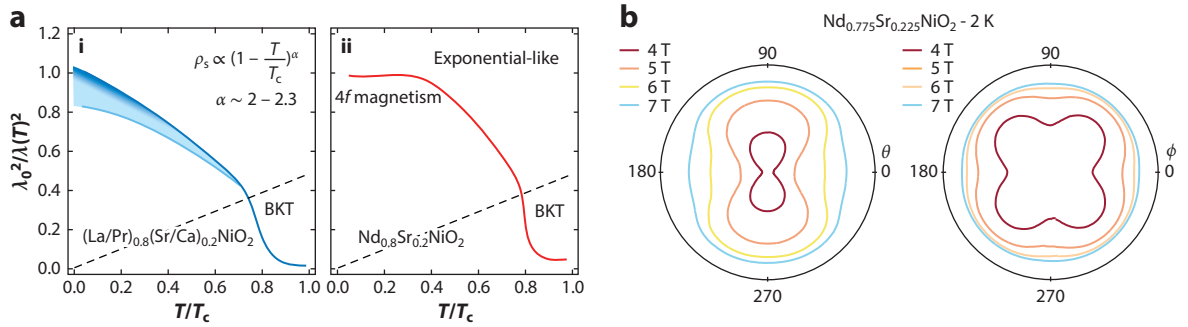


**Figure 4**

(a) Illustration of the temperature dependence of  $n_s$  observed in (i) (La/Pr, Sr/Ca)NiO<sub>2</sub> and (ii) (Nd, Sr)NiO<sub>2</sub> based on experimental measurements (54, 110). The  $n_s$  of La- and Pr-nickelates follows a power-law temperature dependence with exponents around 2, whereas the  $n_s$  of Nd-nickelate exhibits an exponential-like saturation at low temperatures (110). The low-temperature saturation and slight downturn have been ascribed to an artifact related to the Nd 4*f* moments (54, 110, 116). (b) Representative polar ( $\theta$ ) and azimuthal ( $\phi$ ) dependence of Nd<sub>0.775</sub>Sr<sub>0.225</sub>NiO<sub>2</sub> magnetoresistance at 2 K. Panel b adapted from Reference 116 (CC BY-NC 4.0). Abbreviation: BKT, Berezinskii–Kosterlitz–Thouless.

(57, 61, 116, 121) (**Figure 4b**). Another feature observed in the mutual inductance measurement is the Berezinskii–Kosterlitz–Thouless (BKT) transition expected in homogeneous thin films in the form of an abrupt change of  $n_s$  occurring at the temperature at which the superfluid stiffness roughly equals the thermal energy (110). This BKT transition temperature is consistent with a superfluid stiffness calculated assuming superconductivity to be stabilized throughout the entire film thickness, again supporting a bulk response description as discussed in Section 2.1.

### 3.3. Length Scale

There are two key length scales that describe the superconducting order parameter. The coherence length  $\xi$  describes the minimum scale for the spatial variation of  $\Delta$ , and magnetic penetration depth  $\lambda$  describes it for the spatial variation of  $\phi$ . Due to the tetragonal crystal structure, both length scales further have two different values corresponding to spatial variations within and perpendicular to the NiO<sub>2</sub> planes. The in-plane coherence length  $\xi_{\parallel}$  of the IL nickelates has been extracted by performing Ginzburg–Landau fits to the temperature dependence of  $H_{c2}$  near  $T_c$ . It is found to be in the range of 3–7 nm (5, 6, 53–58), as summarized in **Figure 5a**. In contrast,  $\xi_{\perp}$  has only been indirectly estimated to be below 1 nm based on the attribution of the observed thermally activated electrical resistance to the motion of in-plane magnetic vortices (53). Although this is consistent with the expected quasi-2D electronic nature and resembles their cuprate analogs, direct experimental confirmation of dimensionality in the nickelates remains a challenge, largely due to the current lack of bulk superconducting samples (Section 2.3).

With in-plane penetration depth  $\lambda_{ab}$  on the order of  $\sim 1 \mu\text{m}$  (110), the nickelate superconductors are classified as strongly type II, hosting broad magnetic vortices (especially in thin film form) with small nonsuperconducting cores, which have been observed by a recent superconducting quantum interference device investigation (125). In contrast, there is so far no attempt at measuring the out-of-plane penetration depth, which most likely would require a breakthrough in the bulk synthesis efforts.

## 4. NORMAL STATE

Superconductivity is an instability of the normal state: As such, a complete description of the superconducting mechanism requires a deep understanding of the normal state. Although most

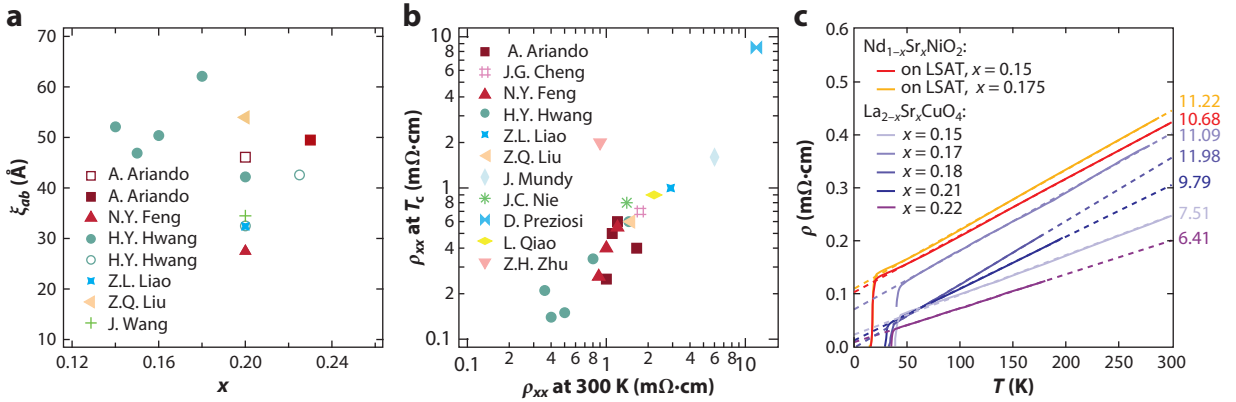


**Figure 5**

(a)  $\xi_{\parallel}$  of various hole-doped infinite-layer nickelates reported so far as a function of hole doping. The solid and open symbols represent La- and Nd-nickelates, respectively. (b) The low-temperature normal state resistivity of the most conductive superconducting nickelate samples in each experimental report so far plotted against their room-temperature resistivity. Legends in panels *a* and *b* denote experimental groups (3–7, 10, 12, 15, 54–56, 58, 60, 61, 64, 65, 86, 92, 112–114). (c) Temperature-dependent resistivity of the Nd-nickelates near optimal doping (10) and the prototypical La<sub>2-x</sub>Sr<sub>x</sub>CuO<sub>4</sub> superconductors (122–124). The linear slopes are labeled on the right in units of  $10^{-4} \text{ m}\Omega \cdot \text{cm} \cdot \text{K}^{-1}$ . Abbreviation: LSAT, (LaAlO<sub>3</sub>)<sub>0.3</sub>(Sr<sub>2</sub>TaAlO<sub>6</sub>)<sub>0.7</sub>.

superconductors have a well-understood Fermi liquid normal state, unconventional superconductors exhibit various unusual behaviors in their normal state, including pseudogap, strange metal, and bad metal transport (105). Whether these properties are also present in the nickelate systems can help guide understanding of the superconducting mechanism.

Bad metal behavior is defined around the Mott–Ioffe–Regel (MIR) limit (111, 126), where coherent quasiparticle conductivity is lost when the mean-free path becomes comparable with the interatomic distance within the crystal lattice. In a typical metal, the electrical resistivity  $\rho$  saturates as it approaches the MIR limit (126, 127). However, in the normal state of unconventional superconductors,  $\rho$  is often observed to substantially exceed this limit as the temperature is increased. Strange metal behavior, another unresolved transport phenomenon of unconventional superconductors, refers to the linear temperature dependence of the resistivity near zero temperature (128, 129), which cannot be satisfactorily explained by the Fermi liquid theory. Bad and strange metal behaviors are considered key transport manifestations of unconventionality in the normal state.

For the IL nickelate superconductors, the MIR limit is estimated to be on the order of  $500 \mu\Omega \cdot \text{cm}$ , with the precise value dependent on the preferred definition (126) and the assumed normal state carrier density (see Section 3.1). Despite a large variation in the normal state resistivity reported in the literature, it is clear in **Figure 5b** that even the most conductive sample has a room-temperature resistivity close to the MIR limit. In parallel, measurements of the optical conductivity observed a broad Drude peak in the normal state (109). The scattering rate extracted from the frequency dependence fit is roughly 37 meV ( $\sim 400$  K), which is substantially greater than the superconducting energy scale. A recent synthesis improvement has also revealed linear-in-temperature resistivity near optimal doping extending from the superconducting transition temperature up to room temperature (10). Although it remains unclear whether such linearity persists to higher temperatures until structural degradation occurs or would persist down to  $T = 0$  if not interrupted by superconductivity, observations to date are in agreement with an unconventional normal state showing signs of both bad metal and strange metal behaviors.

By suppressing the superconductivity with strong magnetic field, Hsu et al. (130, 131) also examined the nonsuperconducting ground state, which is closely related to—if not of the same nature as—the normal state. A persistent correlated insulating behavior is observed, which appears to be a continuation of the disorder-insensitive resistive upturn found in the nonsuperconducting underdoped IL nickelates. Intriguingly, this correlated upturn is maximally suppressed near the optimal doping, around where linear-in-temperature resistivity and the temperature-driven Hall coefficient sign change both emerge. It remains unclear whether such concurrence is coincidental or carries deeper implications.

## 5. OTHER PARTS OF THE PHASE DIAGRAM

Based on the current understanding of the hole-doped phase diagram of the nickelate superconductors (5, 10, 12, 13), superconductivity is but one of several ground states that emerge upon carrier doping. In addition to the hole-doped superconducting dome, understanding the nature of the neighboring ground states and ordered phases in the undoped ( $x = 0$ ), underdoped ( $0 < x \lesssim 0.1$ ), and overdoped ( $0.3 \lesssim x$ ) regions of the doping phase diagram is therefore crucial for deciphering the emergence of superconductivity and developing a comprehensive description of any potential intertwined orders. Given the sample geometry limitations, many of the techniques used to investigate these ordered phases in the cuprates (e.g., surface-sensitive techniques such as scanning tunneling microscopy and ARPES or high-sensitivity bulk techniques such as neutron scattering) are not immediately suitable for the existing nickelate samples. Still, a number of studies have been conducted by X-ray spectroscopy and scattering, transport, nuclear magnetic resonance, and muon spin rotation/relaxation ( $\mu$ SR) experiments probing possible additional—particularly magnetic, charge-density wave, and nematic—orders and other effects.

The undoped parent compound in particular has drawn much attention due to characteristics that stand in contrast to its cuprate counterpart. At zero doping, a metallic resistivity is seen down to roughly 50 K, below which an insulating upturn with a  $\log(T)$ -like temperature dependence is seen (**Figure 6a,b**). At temperatures below 10 K, traces of a superconductivity-like resistivity drop have been reported (5). The underdoped region has a similar temperature dependence of  $\rho$  as the undoped compound, except for the rapid disappearance of the weak resistive downturn mentioned above and a gradual decrease of the metal-insulator transition temperature from  $\sim 50$  K at zero doping to  $\sim 10$  K at around  $x = 0.10$  doping (10). The Hall coefficient in these low-doping regions also has a dramatic nonmonotonic temperature dependence while maintaining a negative (electron-like) value (**Figure 6b**) (10, 12, 13). Although this behavior has persisted even with considerable sample improvements (10), no theoretical models have been able to satisfactorily capture these temperature-dependent transport properties, which are also in contrast to the completely insulating behavior (132) and positive Hall coefficients in underdoped cuprates (133, 134).

Concerning the nature of the resistive upturn in the undoped and underdoped regions, there are currently two primary schools of thought. One perspective draws attention toward the  $\log(T)$  temperature dependence of the resistive upturn, the  $1 - T^2$  resistance saturation at low temperatures, and a nontrivial field suppression of the upturn, motivating a Kondo-impurity-based interpretation (114, 135). The  $\log(T)$  downturn of the Hall coefficient is further interpreted as a natural consequence of the incoherent skew scattering by localized magnetic impurities (114, 136). The other perspective points out the intriguing similarities in the functional temperature dependencies of the resistive upturn and the Hall coefficient drop, which is attributed to a decrease in the contribution to electronic transport by one type of carrier (10). This draws parallels with the observation of charge ordering, which also disappears upon further hole doping. Either

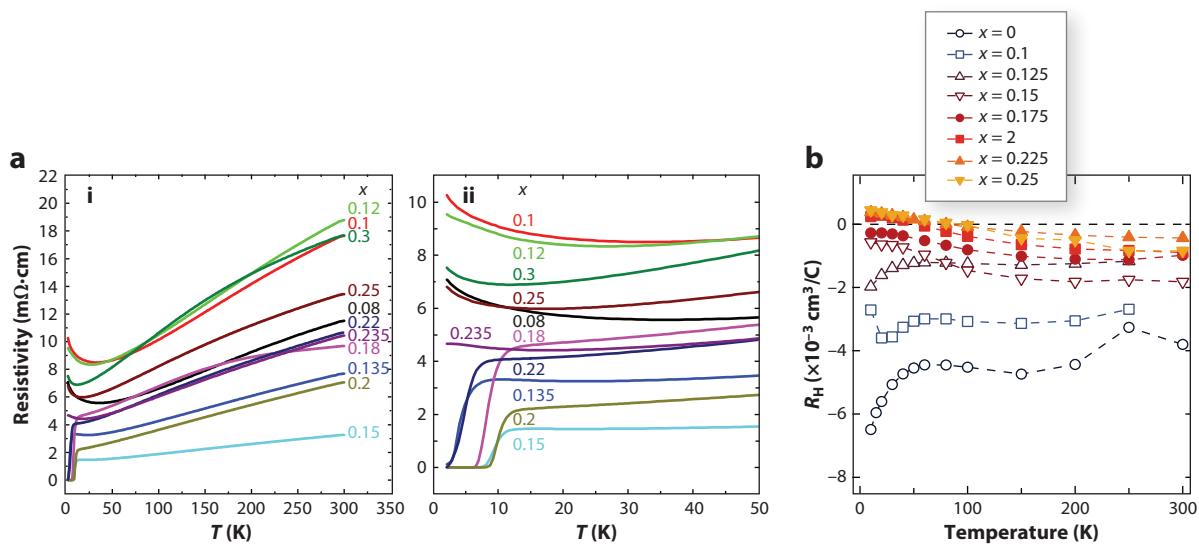


**Figure 6**

(a) Resistivity curves of Nd-nickelate samples with Sr dopings from  $x = 0.08$ – $0.30$  plotted against temperatures from (i) 0 to 300 K and (ii) 0 to 50 K. (b) Hall coefficient versus temperature data of Nd-nickelate samples with Sr dopings from  $x = 0$ – $0.25$ . Panel a adapted with permission from Reference 13. Panel b adapted with permission from Reference 12.

proposal, if true, has significant implications for the superconducting mechanism, and both await further experimental examination.

In the overdoped region, the layered nickelates behave more similarly to disordered metals with clear  $T^2$  temperature dependence at low temperatures until a small resistive upturn appears below 5 K (10). Contrary to the upturn seen in the underdoped region, this upturn exhibits a clear dependence on disorder level and is suppressed upon sample quality improvement (10, 12). The Hall coefficient also develops a temperature-dependent sign crossover for doping levels  $x \gtrsim 0.15$ . The doping-driven Hall sign change at low temperatures, where isotropic defect scattering likely dominates, could be associated with the underlying evolution of fermiology against hole doping, whereas the temperature-driven Hall sign change could be related to the temperature dependence of different scattering mechanisms. Thus far, despite several efforts (43, 136, 137), a satisfactory theoretical description of the Hall coefficient is still missing.

The exact nature of magnetic order in the IL nickelates is still an open question under active investigation. Thus far, no long-range magnetic order has been observed in undoped bulk single crystals, polycrystalline powders, or thin films (77, 78, 138, 139), despite observations of magnon-like dispersions in NdNiO<sub>2</sub> and PrNiO<sub>2</sub> thin films, which are suppressed upon hole doping (16, 140) (Figure 7). Evidence for short-range magnetic order has been observed in all IL compounds across both R and doping series (138, 139, 141, 142). Fowle et al. (141) draw a comparison between glassiness of observed order and the spin-glass state in some cuprates, but they point out that in the nickelates this behavior persists to much higher temperatures, perhaps in closer parallel to the iron pnictides. However, two studies extracting the intrinsic susceptibility in undoped LaNiO<sub>2</sub> report non-Curie-Weiss-like behavior in LaNiO<sub>2</sub> similar to that in underdoped cuprates (138, 143). In parallel, extrinsic structural factors such as crystallinity limitations and sample geometry have been shown to affect the stabilization of ordered phases (14, 15). These initial experimental investigations present interesting implications and call for further understanding of the magnetic

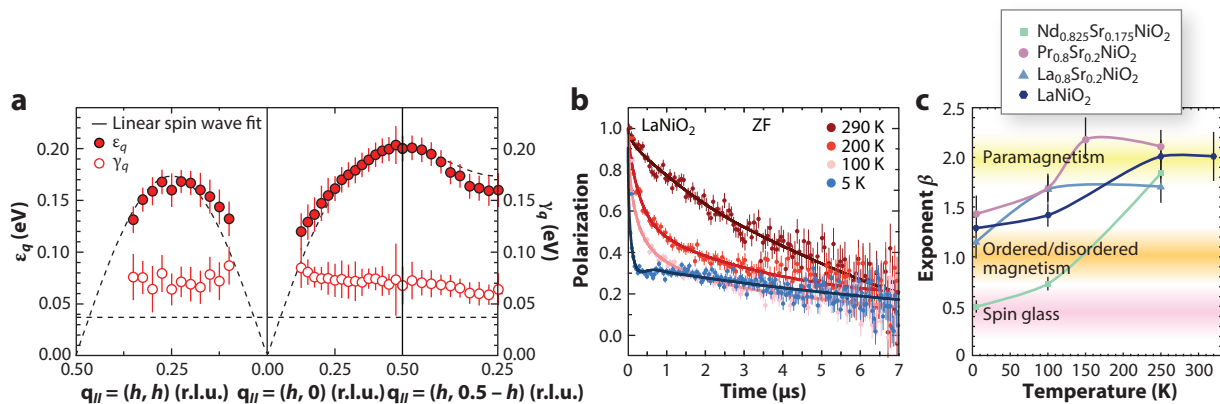


**Figure 7**

(a) Magnetic excitation dispersion in an  $\text{NdNiO}_2$  thin film extracted from resonant inelastic X-ray scattering measurements showing the magnetic mode energy  $\epsilon_q$  and damping factor  $\gamma_q$ . (b) Temperature-dependent zero-field  $\mu$ SR spectra of  $\text{LaNiO}_2$  suggest the presence of short-range order below  $\sim 75$  K while exhibiting no signatures of long-range order. (c) Summary of different forms of magnetism across the infinite-layer nickelate series based on  $\mu$ SR analysis. Panel a adapted with permission from Reference 16; copyright 2021 AAAS. Panel b adapted from Reference 138 (CC BY 4.0). Panel c adapted with permission from Reference 141. Abbreviation: ZF, zero field.

order and its role in superconductivity in the nickelates, which could also shed light on the much debated role of magnetism in cuprate superconductivity.

Signatures of charge order measured by resonant X-ray scattering have also been reported in undoped and underdoped IL compounds of all three R species (La, Pr, and Nd) (11, 14, 15, 144). The first report of short-range stripe-like order in  $(\text{La,Sr})\text{NiO}_2$  with incommensurate in-plane wave vector  $Q \approx (0.344, 0)$  diminishing with Sr substitution toward optimal hole doping (11) (Figure 8) was followed by measurements of  $\text{PrNiO}_2$  indicating an additional out-of-plane component to the charge-order vector,  $Q \approx (1/3, 0, 0.365)$  (144). In Nd-nickelate films, resonant X-ray signatures of commensurate in-plane order with  $Q = (1/3, 0)$  were linked to the direct

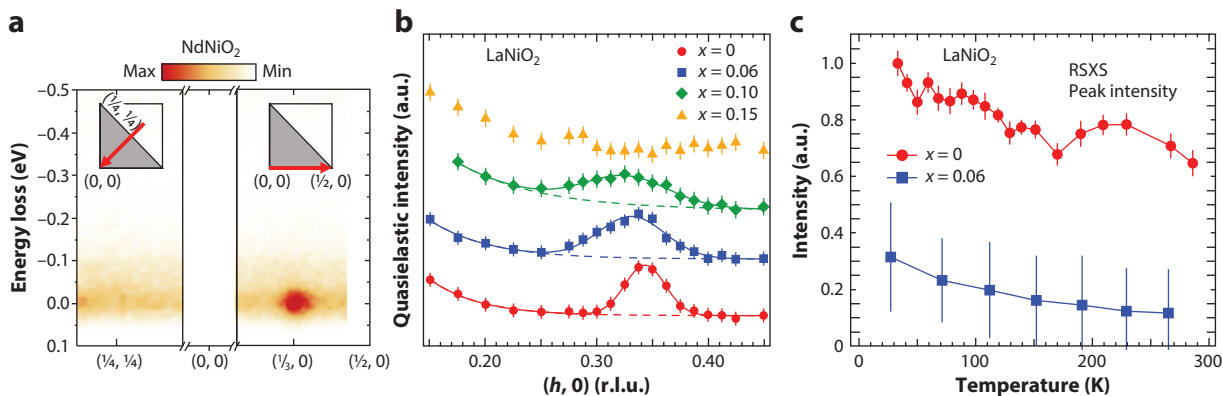


**Figure 8**

(a) In-plane momentum scattering intensity maps of an  $\text{NdNiO}_2$  film along the high-symmetry directions indicated by the insets. (b) Extracted intensity of the RIXS charge-order peak for different doping levels in  $\text{La}_{1-x}\text{Sr}_x\text{NiO}_2$  thin films. (c) Temperature dependence of the RSXS charge-order peak for an undoped ( $x = 0$ ) and lightly doped ( $x = 0.06$ )  $\text{La}_{1-x}\text{Sr}_x\text{NiO}_2$  thin films. Panel a adapted from Reference 15. Panels b and c adapted with permission from Reference 11. Abbreviations: RIXS, resonant inelastic X-ray scattering; RSXS, resonant soft X-ray scattering.

real-space observation of excess oxygen ordered in locally off-stoichiometric phases, NdNiO<sub>2+δ</sub> (145, 146), but it is unclear at the moment if this is true for all R series of the IL nickelates given the sensitivity of ordered phases to chemical or structural perturbations such as strain. If charge order is indeed intrinsic in certain IL nickelates, the direction of the ordering vector could explain the lack of observed antiferromagnetic (AFM) order that would form along the  $Q = (b, b)$  direction (11, 14), pointing to competition between these two phases. Compared to the cuprates, in which charge order emerges only upon doping away from the half-filled formal  $d^9$  configuration, the presence and robustness of charge order in undoped nickelates would be consistent with self-doping effects in the metallic parent compounds (11, 14, 32, 37, 46, 136). In this sense, the nickelate parent compound is never strictly undoped, which could also explain the suppression of the expected AFM Mott insulator ground state and the superconductivity-like transport features (5).

As mentioned in Section 2.4, the possibility that excess oxygen may also contribute some hole doping away from the nominal value set by cation substitution is still not ruled out, although the qualitative trends have been thus far reproducible among different groups with different synthesis recipes. Also currently in question is the potential impact of a capping layer on the presence of charge order in nickelate films: Rossi et al. and Ren et al. report charge order in capped La<sub>1-x</sub>Sr<sub>x</sub>NiO<sub>2</sub> (11) and PrNiO<sub>2</sub> (144) films, respectively, whereas Tam et al. (14) and Krieger et al. (15) report charge order only in uncapped NdNiO<sub>2</sub> films (charge order is absent in their capped films). The impact of intrinsic versus extrinsic effects, such as varying degrees of crystalline order in films with or without capping layers, in these observations remains to be understood: Detailed investigation of the film-capping layer interface did not reveal any distinct electronic modification compared to the substrate-film interface, which is present in all thin films (74), but future studies to systematically compare between samples produced by different groups may offer some clarifications in this regard.

## 6. SUMMARY AND OUTLOOK

Clearly, though the nickelates appear closely analogous to the cuprates in many aspects, there are notable distinctions that position these compounds as a fascinating materials family in their own right with several outstanding questions to be addressed (see **Table 1**). In general, there should be a concrete establishment of an overall phase diagram in these materials—by either hole (or electron) doping or formal  $d$  electron count—with a basic classification of the ground state. More

**Table 1** Summary of nickelate properties

Properties	Value/character	References	Notes
$T_c$	$\lesssim 23$ K	5–7, 10, 12, 13, 147	Lower than cuprates
$J_c$	$\sim 300$ kA/cm <sup>2</sup>	3, 4, 58	Lower than cuprates
$H_{c2}$	$\lesssim 35$ T	3, 6, 53, 55–58	Lower than cuprates
$\xi_{\parallel}$	3–7 nm	3, 5, 6, 53–58	Similar to cuprates
$\lambda_{ab}$	$\sim 1$ $\mu$ m	54, 110	Larger than cuprates
Gap symmetry	Nodal (?)	54, 69, 110	Same as cuprates
$n_{\text{normal state}}$	$\sim 0.2\text{--}2.5$ u.c. <sup>-1</sup> (?)	10, 12, 13	Same order as cuprates
$\rho_{300\text{K}}$	$\sim 1$ m $\Omega$ ·cm	5–7, 10, 12, 13, 147	Larger than cuprates, exceeds MIR limit
$\rho_{20\text{K}}$	$\sim 100$ $\mu\Omega$ ·cm	5–7, 10, 12, 13, 147	Larger than cuprates
Magnetic order	Short-range AFM (?)	11, 15, 16, 141	Persists to high temperatures, similar to iron pnictides
Charge order	Short-range stripe order (?)	11, 14, 15, 145	Similar to underdoped cuprates

Abbreviations: AFM, antiferromagnetic; MIR, Mott–Ioffe–Regel; (?), indicates parameters that require further investigation.

specifically, measurements or estimates of fundamental properties including electrical resistivity, carrier density, scattering mechanisms, and magnetoresistance are desired. Other probes of dimensionality and anisotropy may also provide useful insights, such as optical conductivity, direct transport, or superconducting coherence length measurements along the  $c$  axis. Eventually, it will be interesting to examine the doping dependence of the band structure and address questions relating to the magnitude of  $U$ , band filling of the doped holes, and the relevance of the R bands across the nickelate family. Basic experimental characterization of the phonon band structure will lay the foundation for optical investigations in the future. The competition between superconductivity and other competing orders (e.g., charge order, magnetism) needs to be more concretely demonstrated across temperatures and doping levels, along with more systematic investigation of both direct and indirect impacts of strain, isotope effect, and disorder.

The most crucial breakthroughs will come with experimental measurements of the band structure and stabilization of superconducting bulk nickelates which will enable  $c$ -axis transport, neutron scattering, magnetic susceptibility, and thermodynamic measurements. Both goals highlight the importance of synthetic advances, which despite recent leaps forward remain a bottleneck for this field. Indeed, materials improvements have in many cases already demonstrated that extrinsic factors relating to crystallinity cannot be treated lightly. As one of many examples, the initial discovery of nickelate superconductivity in Nd-compounds noted its absence in doped La-compounds (3). Although this distinction spurred some early discussion about fundamental differences between the two R species, in the span of two years it became clear that the initial lack of La-superconductivity was due to limited sample quality in early specimens (5, 6). In order to avoid future affliction by “Inverse Occam’s Razor” (148), it is crucial that the material synthesis advances in parallel with the growing physical understanding of this system, and that any new physical understanding takes into careful account the contemporary synthetic reality of the investigated samples. Transparent metrics of both local and global crystalline quality, for example, by X-ray diffraction and transmission electron microscopy, should be consistently reported along with other experimental measurements. When possible, experimental measurements should also be duplicated and samples shared among groups, particularly with the successful demonstration of diverse synthetic recipes. In spite of these challenges, the long and winding road to nickelate superconductivity now boasts promising opportunities to make strides toward the fundamental understanding of unconventional superconductivity.

## DISCLOSURE STATEMENT

The authors are not aware of any affiliations, memberships, funding, or financial holdings that might be perceived as affecting the objectivity of this review.

## ACKNOWLEDGMENTS

The authors thank Danfeng Li, Chaitanya Murthy, and Gaël Grissonnanche for useful discussions. B.H.G. acknowledges support from the Schmidt Science Fellows in partnership with the Rhodes Trust. B.Y.W. and K.L. acknowledge support from the US Department of Energy, Office of Basic Energy Sciences, Division of Materials Sciences and Engineering (contract DE-AC02-76SF00515).

## LITERATURE CITED

1. Bednorz JG, Müller KA. 1986. *Z. Phys. B Condens. Matter* 64(2):189–93
2. Anisimov VI, Bukhvalov D, Rice TM. 1999. *Phys. Rev. B* 59(12):7901–6
3. Li D, Lee K, Wang BY, Osada M, Crossley S, et al. 2019. *Nature* 572(7771):624–27

4. Osada M, Wang BY, Goodge BH, Lee K, Yoon H, et al. 2020. *Nano Lett.* 20(8):5735–40
5. Osada M, Wang BY, Goodge BH, Harvey SP, Lee K, et al. 2021. *Adv. Mater.* 33(45):2104083
6. Zeng S, Li C, Chow LE, Cao Y, Zhang Z, et al. 2022. *Sci. Adv.* 8(7):eabl9927
7. Pan GA, Ferenc Segedin D, LaBollita H, Song Q, Nica EM, et al. 2022. *Nat. Mater.* 21(2):160–64
8. Ferenc Segedin D, Goodge BH, Pan GA, Song Q, LaBollita H, et al. 2023. *Nat. Commun.* 14:1468
9. Mitchell J. 2021. *Front. Phys.* 9:813483
10. Lee K, Wang BY, Osada M, Goodge BH, Wang TC, et al. 2023. *Nature* 619:288–92
11. Rossi M, Osada M, Choi J, Agrestini S, Jost D, et al. 2022. *Nat. Phys.* 18:869–873
12. Li D, Wang BY, Lee K, Harvey SP, Osada M, et al. 2020. *Phys. Rev. Lett.* 125(2):027001. <https://doi.org/10.1103/PhysRevLett.125.027001>
13. Zeng S, Tang CS, Yin X, Li C, Li M, et al. 2020. *Phys. Rev. Lett.* 125(14):147003. <https://doi.org/10.1103/PhysRevLett.125.147003>
14. Tam CC, Choi J, Ding X, Agrestini S, Nag A, et al. 2022. *Nat. Mater.* 21(10):1116–20
15. Krieger G, Martinelli L, Zeng S, Chow L, Kummer K, et al. 2022. *Phys. Rev. Lett.* 129(2):027002
16. Lu H, Rossi M, Nag A, Osada M, Li D, et al. 2021. *Science* 373(6551):213–16
17. Lee KW, Pickett WE. 2004. *Phys. Rev. B* 70(16):165109
18. Botana AS, Bernardini F, Cano A. 2021. *J. Exp. Theor. Phys.* 132:618–27
19. Norman MR. 2020. *Physics* 13:85
20. Chow LE, Ariando A. 2022. *Front. Phys.* 10:20
21. Ji Y, Liu J, Li L, Liao Z. 2021. *J. Appl. Phys.* 130(6):060901
22. Nomura Y, Arita R. 2022. *Rep. Prog. Phys.* 85(5):052501
23. Pickett WE. 2021. *Nat. Rev. Phys.* 3:7–8
24. Zhang J, Tao X. 2021. *CrystEngComm* 23(18):3249–64
25. Gu Q, Wen H. 2022. *Innovation* 3:100202
26. Yang X, Li M, Ding Z, Li L, Ji C, Wu G. 2023. *Adv. Quantum Technol.* 6:2200065
27. Zhou X, Qin P, Feng Z, Yan H, Wang X, et al. 2022. *Mater. Today* 55:170–85
28. Zaanen J, Sawatzky GA, Allen JW. 1985. *Phys. Rev. Lett.* 55(4):418–21
29. Hu LH, Wu C. 2019. *Phys. Rev. Res.* 1(3):032046
30. Jiang M, Berciu M, Sawatzky GA. 2020. *Phys. Rev. Lett.* 124(20):207004
31. Hirayama M, Tadano T, Nomura Y, Arita R. 2020. *Phys. Rev. B* 101(7):075107
32. Karp J, Botana AS, Norman MR, Park H, Zingl M, Millis A. 2020. *Phys. Rev. X* 10(2):021061
33. Hepting M, Li D, Jia CJ, Lu H, Paris E, et al. 2020. *Nat. Mater.* 19(4):381–85
34. Goodge BH, Li D, Lee K, Osada M, Wang BY, et al. 2021. *PNAS* 118(2):e2007683118
35. Chen Z, Osada M, Li D, Been EM, Chen SD, et al. 2022. *Matter* 5(6):1806–15
36. Rossi M, Lu H, Nag A, Li D, Osada M, et al. 2021. *Phys. Rev. B* 104(22):L220505. <https://doi.org/10.1103/PhysRevB.104.L220505>
37. Botana AS, Norman MR. 2020. *Phys. Rev. X* 10:011024
38. Kitatani M, Si L, Janson O, Arita R, Zhong Z, Held K. 2020. *npj Quantum Mater.* 5:59
39. Been E, Lee WS, Hwang HY, Cui Y, Zaanen J, et al. 2021. *Phys. Rev. X* 11:011050
40. Gao J, Peng S, Wang Z, Fang C, Weng H. 2021. *Natl. Sci. Rev.* 8(8):nwaa218
41. Bernardini F, Olevano V, Cano A. 2020. *Phys. Rev. Res.* 2:013219
42. Ryee S, Yoon H, Kim TJ, Jeong MY, Han MJ. 2020. *Phys. Rev. B* 101(6):064513
43. Leonov I, Skornyakov S, Savrasov S. 2020. *Phys. Rev. B* 101(24):241108
44. Liu Z, Xu C, Cao C, Zhu W, Wang Z, Yang J. 2021. *Phys. Rev. B* 103(4):045103
45. Lechermann F. 2021. *Phys. Rev. Mater.* 5(4):044803
46. Lechermann F. 2020. *Phys. Rev. B* 101(8):081110
47. Nomura Y, Hirayama M, Tadano T, Yoshimoto Y, Nakamura K, Arita R. 2019. *Phys. Rev. B* 100(20):205138
48. Werner P, Hoshino S. 2020. *Phys. Rev. B* 101(4):041104
49. Olevano V, Bernardini F, Blase X, Cano A. 2020. *Phys. Rev. B* 101(16):161102
50. Wu X, Di Sante D, Schwemmer T, Hanke W, Hwang HY, et al. 2020. *Phys. Rev. B* 101(6):060504
51. Sakakibara H, Usui H, Suzuki K, Kotani T, Aoki H, Kuroki K. 2020. *Phys. Rev. Lett.* 125(7):077003

52. Zhang F, Rice T. 1988. *Phys. Rev. B* 37(7):3759
53. Wang BY, Li D, Goodge BH, Lee K, Osada M, et al. 2021. *Nat. Phys.* 17(4):473–77
54. Chow LE, Sudheesh SK, Nandi P, Zeng S, Zhang Z, et al. 2022. arXiv:2201.10038
55. Sun W, Li Y, Liu R, Yang J, Li J, et al. 2023. *Adv. Mater.* 35(32):2303400
56. Ji Y, Liu J, Gao X, Li L, Chen K, Liao Z. 2023. *Phys. C Supercond. Appl.* 604:1354190
57. Ji H, Liu Y, Li Y, Ding X, Xie Z, et al. 2023. *Nat. Commun.* 14:7155
58. Zhou XR, Feng ZX, Qin PX, Yan H, Wang XN, et al. 2021. *Rare Metals* 40(10):2847–54
59. Ortiz RA, Menke H, Misják F, Mantadakis DT, Fürsich K, et al. 2021. *Phys. Rev. B* 104(16):165137
60. Zeng S, Yin X, Li C, Chow L, Tang C, et al. 2022. *Nat. Commun.* 13:743
61. Chow LE, Rubi K, Yip KY, Pierre M, Leroux M, et al. 2023. arXiv:2301.07606
62. Kawai M, Matsumoto K, Ichikawa N, Mizumaki M, Sakata O, et al. 2010. *Crystal Growth Des.* 10(5):2044–46
63. Lee K, Goodge BH, Li D, Osada M, Wang BY, et al. 2020. *APL Mater.* 8(4):041107
64. Li Y, Sun W, Yang J, Cai X, Guo W, et al. 2021. *Front. Phys.* 9:719534
65. Gao Q, Zhao Y, Zhou X, Zhu Z. 2021. *Chin. Phys. Lett.* 38(7):077401
66. Onozuka T, Chikamatsu A, Katayama T, Fukumura T, Hasegawa T. 2016. *Dalton Trans.* 45(30):12114–18
67. Kawai M, Inoue S, Mizumaki M, Kawamura N, Ichikawa N, Shimakawa Y. 2009. *Appl. Phys. Lett.* 94(8):082102
68. Li H, Hao P, Zhang J, Gordon K, Linn AG, et al. 2023. *Sci. Adv.* 9(2):eade4418
69. Gu Q, Li Y, Wan S, Li H, Guo W, et al. 2020. *Nat. Commun.* 11:6027
70. Wang RF, Xiong YL, Yan H, Hu X, Osada M, et al. 2023. *Phys. Rev. B* 107(11):115411
71. Wang BX, Zheng H, Krivyakina E, Chmaissem O, Lopes PP, et al. 2020. *Phys. Rev. Mater.* 4(8):084409
72. Puphal P, Wu YM, Fürsich K, Lee H, Pakdaman M, et al. 2021. *Sci. Adv.* 7(49):eabl8091
73. Puphal P, Wehinger B, Nuss J, Küster K, Starke U, et al. 2023. *Phys. Rev. Mater.* 7:014804
74. Goodge BH, Geisler B, Lee K, Osada M, Wang BY, et al. 2023. *Nat. Mater.* 22:466–73
75. Catalano S, Gibert M, Fowlie J, Iniguez J, Triscone JM, Kreisel J. 2018. *Rep. Prog. Phys.* 81(4):046501
76. Crespin M, Levitz P, Gatineau L. 1983. *J. Chem. Soc. Faraday Trans. 2 Mol. Chem. Phys.* 79(8):1181–94
77. Hayward MA, Green MA, Rosseinsky MJ, Sloan J. 1999. *J. Am. Chem. Soc.* 121(38):8843–54
78. Hayward M, Rosseinsky M. 2003. *Solid State Sci.* 5:839–50
79. Kaneko D, Yamagishi K, Tsukada A, Manabe T, Naito M. 2009. *Phys. C Supercond.* 469(15–20):936–39
80. Moriga T, Usaka O, Nakabayashi I, Kinouchi T, Kikkawa S, Kanamaru F. 1995. *Solid State Ion.* 79:252–55
81. Wei W, Shin K, Hong H, Shin Y, Thind AS, et al. 2023. *Phys. Rev. Mater.* 7:013802
82. Fürsich K, Pons R, Bluschke M, Ortiz R, Wintz S, et al. 2022. *Front. Phys.* 9:793
83. Ando Y, Segawa K. 2002. *Phys. Rev. Lett.* 88(16):167005
84. Yu Y, Ma L, Cai P, Zhong R, Ye C, et al. 2019. *Nature* 575(7781):156–63
85. Segedin DF, Goodge BH, Pan GA, Song Q, LaBollita H, et al. 2023. *Nat. Commun.* 14:1468
86. Ren X, Li J, Chen W-C, Gao Q, Sanchez JJ, et al. 2021. arXiv:2109.05761v3
87. Li Q, He C, Si J, Zhu X, Zhang Y, Wen HH. 2020. *Commun. Mater.* 1:16
88. He C, Ming X, Li Q, Zhu X, Si J, Wen HH. 2021. *J. Phys. Condens. Matter* 33(26):265701
89. Geisler B, Pentcheva R. 2020. *Phys. Rev. B* 102(2):020502
90. He R, Jiang P, Lu Y, Song Y, Chen M, et al. 2020. *Phys. Rev. B* 102(3):035118
91. Ikeda A, Krockenberger Y, Irie H, Naito M, Yamamoto H. 2016. *Appl. Phys. Express* 9(6):061101
92. Wang N, Yang M, Yang Z, Chen K, Zhang H, et al. 2022. *Nat. Commun.* 13:4367
93. Si L, Xiao W, Kaufmann J, Tomczak JM, Lu Y, et al. 2020. *Phys. Rev. Lett.* 124(16):166402
94. Si L, Worm P, Held K. 2022. *Crystals* 12(5):656
95. Malý OI, Varignon J, Zunger A. 2022. *Phys. Rev. B* 105:014106
96. Ding X, Tam CC, Sui X, Zhao Y, Xu M, et al. 2023. *Nature* 615(7950):50–55
97. Moodenbaugh A, Xu Y, Suenaga M, Folkerts T, Shelton R. 1988. *Phys. Rev. B* 38(7):4596
98. Tranquada J, Sternlieb B, Axe J, Nakamura Y, Uchida S. 1995. *Nature* 375(6532):561–63
99. Chaloupka J, Khaliullin G. 2008. *Phys. Rev. Lett.* 100:016404
100. Hansmann P, Yang X, Toschi A, Khaliullin G, Andersen O, Held K. 2009. *Phys. Rev. Lett.* 103:016401
101. Han MJ, Wang X, Marianetti C, Millis A. 2011. *Phys. Rev. Lett.* 107(20):206804

102. Lacorre P. 1992. *J. Solid State Chem.* 97(2):495–500
103. Zhang J, Botana A, Freeland J, Phelan D, Zheng H, et al. 2017. *Nat. Phys.* 13(9):864–69
104. Nica EM, Krishna J, Yu R, Si Q, Botana AS, Erten O. 2020. *Phys. Rev. B* 102(2):020504
105. Keimer B, Kivelson SA, Norman MR, Uchida S, Zaanen J. 2015. *Nature* 518(7538):179–86
106. Si Q, Steglich F. 2010. *Science* 329(5996):1161–66
107. Grewe N, Steglich F. 1991. *Handb. Phys. Chem. Rare Earths* 14:343–474
108. Emery V, Kivelson S. 1995. *Nature* 374:434–37
109. Cervasio R, Tomarchio L, Verseils M, Brubach JB, Macis S, et al. 2023. *ACS Appl. Electron. Mater.* 5(9):4770–77
110. Harvey SP, Wang BY, Fowlie J, Osada M, Lee K, et al. 2022. arXiv:2201.12971
111. Emery V, Kivelson S. 1995. *Phys. Rev. Lett.* 74(16):3253
112. Xiang Y, Li Q, Li Y, Yang H, Nie Y, Wen HH. 2021. *Chin. Phys. Lett.* 38(4):047401
113. Ding X, Shen S, Leng H, Xu M, Zhao Y, et al. 2022. *Sci. China Phys. Mech. Astron.* 65(6):267411
114. Shao T, Zhang Z, Qiao Y, Zhao Q, Liu H, et al. 2022. arXiv:2209.06400
115. Tinkham M. 2004. *Introduction to Superconductivity*. Minneola, NY: Dover Publ.
116. Wang BY, Wang TC, Hsu YT, Osada M, Lee K, et al. 2023. *Sci. Adv.* 9(20):eadf6655
117. Clogston AM. 1962. *Phys. Rev. Lett.* 9(6):266
118. Chandrasekhar B. 1962. *Appl. Phys. Lett.* 1:7–8
119. Saito Y, Nojima T, Iwasa Y. 2017. *Nat. Rev. Mater.* 2:16094
120. Chow L, Yip K, Pierre M, Zeng S, Zhang Z, et al. 2022. arXiv:2204.12606
121. Krieger G, Raji A, Schlur L, Versini G, Bouillet C, et al. 2022. *J. Phys. D Appl. Phys.* 56(2):024003
122. Takagi H, Batlogg B, Kao H, Kwo J, Cava RJ, et al. 1992. *Phys. Rev. Lett.* 69(20):2975–78
123. Boebinger G, Ando Y, Passner A, Kimura T, Okuya M, et al. 1996. *Phys. Rev. Lett.* 77(27):5417–20
124. Cooper R, Wang Y, Vignolle B, Lipscombe O, Hayden S, et al. 2009. *Science* 323(5914):603–7
125. Shi R, Lee K, Wang BY, Iguchi Y, Hwang H, Moler K. 2023. *Bull. Am. Phys. Soc.* 68(3):S19.00006 (Abstr.)
126. Hussey N, Takenaka K, Takagi H. 2004. *Philos. Mag.* 84(27):2847–64
127. Gunnarsson O, Calandra M, Han J. 2003. *Rev. Mod. Phys.* 75(4):1085
128. Gurvitch M, Fiory A. 1987. *Phys. Rev. Lett.* 59(12):1337–40
129. Phillips PW, Hussey NE, Abbamonte P. 2022. *Science* 377(6602):eabh4273
130. Hsu YT, Wang BY, Berben M, Li D, Lee K, et al. 2021. *Phys. Rev. Res.* 3(4):L042015
131. Hsu YT, Osada M, Wang B, Berben M, Duffy C, et al. 2022. *Front. Phys.* 10:846639
132. Takagi H, Ido T, Ishibashi S, Uota M, Uchida S, Tokura Y. 1989. *Phys. Rev. B* 40(4):2254–61
133. Suzuki M. 1989. *Phys. Rev. B* 39(4):2312–21
134. Hwang H, Batlogg B, Takagi H, Kao H, Kwo J, et al. 1994. *Phys. Rev. Lett.* 72(16):2636–39
135. Yang Yf, Zhang GM. 2022. *Front. Phys.* 9:783
136. Zhang GM, Yang YF, Zhang FC. 2020. *Phys. Rev. B* 101(2):020501
137. Bötzel S, Eremin IM, Lechermann F. 2023. *Phys. Rev. B* 107:174526
138. Ortiz RA, Puphal P, Klett M, Hotz F, Kremer RK, et al. 2022. *Phys. Rev. Res.* 4(2):023093
139. Lin H, Gawryluk DJ, Klein YM, Huangfu S, Pomjakushina E, et al. 2022. *N. J. Phys.* 24:013022
140. Gao Q, Fan S, Wang Q, Li J, Ren X, et al. 2022. arXiv:2208.05614
141. Fowlie J, Hadjimichael M, Martins MM, Li D, Osada M, et al. 2022. *Nat. Phys.* 18(9):1043–47
142. Cui Y, Li C, Li Q, Zhu X, Hu Z, et al. 2021. *Chin. Phys. Lett.* 38(6):067401
143. Zhao D, Zhou Y, Fu Y, Wang L, Zhou X, et al. 2021. *Phys. Rev. Lett.* 126(19):197001
144. Ren X, Sutarto R, Gao Q, Wang Q, Li J, et al. 2023. arXiv:2303.02865
145. Raji A, Krieger G, Viart N, Preziosi D, Rueff J-P, Gloter A. 2023. *Small* 19(49):2304872
146. Parzyck CT, Gupta NK, Wu Y, Anil V, Bhatt L, Bouliane M, et al. 2023. arXiv:2307.06486
147. Wei W, Sun W, Sun Y, Jin G, Yang F, et al. 2023. *Phys. Rev. B* 107: L220503
148. Mazin I. 2022. *Nat. Phys.* 18(4):367–68